RESEARCH PAPER

An XYZ micromanipulator for precise positioning applications

Mohammadali Ghafarian[1] ⓘ · **Bijan Shirinzadeh**[1] · **Ammar Al-Jodah**[1] · **Tilok Kumar Das**[1] · **Weichen Wei**[1] ·
Yanling Tian[2] · **Dawei Zhang**[3]

Abstract

A three-degrees-of-freedom (3-DOF) monolithic compliant parallel micromanipulator with bridge-type displacement amplifier is presented in this paper. The research aims are to design a monolithic mechanism with capability of working in three translational axes and having a high resonant frequency. As a result of being precise in rotation, circular flexure hinges are adopted in the structure of the proposed mechanism and its corresponding mathematical modeling is investigated. A finite element analysis (FEA) model is developed to perform analysis and predict the behaviour of the proposed mechanism and the utilized amplifier, and thus establish the computational Jacobian, workspace and amplification ratio. The stress-strain relationship of the proposed mechanism is investigated by applying safety factor and the results are presented. Finally, an experimental study is conducted to evaluate the dynamic and tracking performances of the proposed flexure-based spatial mechanism. A feedback Proportional-Integral (PI) control methodology is implemented to enhance the mechanism positioning performance and eliminate hysteresis effect inherent in piezoelectric actuators. Based on the designed parameters, the proposed manipulator can have a large workspace, high band-width frequency, and fine tracking resolution along each working axes.

Keywords Monolithic structure · Compliant parallel micromanipulator · Three translational DOF ·
Three Prismatic-Universal-Universal (PUU) flexure-based micromanipulator

1 Introduction

Micro/Nano manipulation is a branch of science focusing on manipulating objects at micro level with nanometre resolution. It has a broad range of applications such as micro-assembly, microsurgery, carbon nanotube (CNT) harvesting, imprint lithography, nano particles manipulation, biotechnology, and many more [1–4]. Many researchers have studied the design and analysis of different types of micromanipulators to accommodate various applications and enhance performance with respect to the needs. Different actuation principles [5–8], amplification mechanisms, dexterity, decoupling pure motions, size of the mechanism, large workspace, and high bandwidth frequency are some of the issues that encourage researchers for designing different micro/nano manipulation mechanisms. Flexure hinges are one of the key aspects in such mechanisms. Because of small thickness of hinges, the combination of different kinds of flexure hinges makes it possible to have different DOF without using any conventional joints. Flexure hinges have some unique advantages such as no friction, noise, backlash, wear and no need for lubrication. As a result, many researchers have focused their attention on designing micro/nano manipulators by using different types of flexure hinges [9–14]. During the past decade, many studies have been focused on different DOF micro/nano manipulation mechanisms. Das et al. [15] investigated a new 2-DOF compliant piezo-driven microgripper capable of grasping and micro positioning of micro-objects. A robust motion tracking control of a 2-DOF flexure-based micro/nanomechanism was presented by Bhagat et al. [16]. Nonlinearities such as creep/drift and hysteresis were compensated with closed-loop control. Yang et al. [17]

✉ Mohammadali Ghafarian
mohammadali.ghafarian@monash.edu

1 Robotics and Mechatronics Research Laboratory (RMRL),
Department of Mechanical and Aerospace Engineering,
Monash University, Melbourne, Australia

2 School of Engineering, University of Warwick, Coventry,
CV4 7AL, UK

3 School of Mechanical Engineering, Tianjin University,
Tianjin, 300072, China

presented the design, analysis and testing of a novel decoupled 2-DOF flexure-based piezo driven micropositioning stage using Scott-Russell and lever mechanisms to enlarge the workspace. Zhu et al. [18] developed a new 2-DOF parallel compliant mechanism for large workspace nanopositioning with decoupled motions incorporating a Z-shaped flexure hinge (ZFH) mechanism. In that design, bridge type mechanism, two-stage lever mechanisms and ZFH mechanism serve as displacement amplifiers.

Due to increasing applications of micromanipulators, the demand for having mechanisms with three and more degrees-of-freedom has escalated drastically. However, the resonant frequency of a micromanipulator is a limitation for specific applications that need high-speed scanning. Regarding that, Bhagat et al. [19] focused on the design and analysis of a novel flexure-based $XY\theta$ mechanism. The introduced mechanism was a non-monolithic structure that caused assembly error and had a low resonant frequency of 489.9 Hz although was made of stiff and good quality material, AL T7075, and being planar. Guo et al. [20] designed a 3-DOF planar monolithic piezo-driven flexure-based mechanism. The mechanical design optimization was conducted to improve the performance of flexure-based mechanism. Unfortunately, the proposed mechanism possessed a low frequency of 357.97 Hz even though the design was optimized to have a good performance and it was manufactured through a very precise manufacturing technique, wire electrical discharge machining (WEDM), using AL T7075. Clark et al. [21] presented the design, optimization, and computational and experimental performance evaluations of a passively actuated, monolithic, compliant $XY\theta$ mechanism. A novel 3-DOF monolithic compliant micropositioning mechanism was presented by Al-Jodah et al. [22]. Analytical and computational analyses were performed while voice coil motor (VCM) was considered as the actuation part. The presented manipulator was in a spatial configuration and was manufactured monolithically using a 3D printing technique and made of Acrylonitrile butadiene styrene (ABS). Additionally, it had a low resonant frequency of 109.37 Hz. Cai et al. [23] investigated an $XY\theta$ stage with T-shape flexure hinges for the applications in the precision measurement equipments and micro/nano manipulation systems. Ding et al. [24] proposed a novel planar 3-DOF micromanipulation stage with large rotational displacement. Wang and Zhang [25] described a general analysis and optimization of a planar parallel 3-DOF nanopositioner. Qin et al. [26] presented a novel planar 3-DOF monolithic manipulator utilizing an improved Scott-Russell mechanism to magnify the displacement of the PEA and increase the workspace. Dong et al. [27] proposed a novel planar micromanipulator, which uses a 3-RPR parallel mechanism. Having parallel mechanism, monolithic and compliant structure, and piezo driven were the characteristics of the

said micromanipulator. The above-mentioned researches were mostly surrounding planar mechanisms capable of performing $XY\theta$ motions. An XYZ mechanism is usually in a spatial configuration and considering this fact, it essentially reduces the resonant frequency of the mechanism in comparison with a planar mechanism. In addition, the kinds of material which are used in the mantufacturing of the manipulator are very important in the resonant frequency of the mechanism. Actually, the material has a direct relationship with the resonant frequency which means the stiffer the material the higher the resonant frequency. A 3-DOF XYZ micromanipulator which was fabricated using surface micromachining processes, was introduced by Jensen et al. [28]. Xu and Li [29] designed an optimized spatial nonmonolithic XYZ nanopositioning piezo-stage. 82 Hz was reported as the first resonant frequency of the proposed design. Tang and Chen [30] proposed a non-monolithic XYZ flexure-based micromanipulator manufactured from AL T7075. The proposed design possessed a very low resonant frequency of 80 Hz, although its material had a large Young's modulus. As a consequence of low bandwidth frequency manicromanipulators which were described above, it can be concluded that there is a need to introduce a design that has the advantages of working in different axes, high resonant frequency, and large workspace.

In this paper, the focus is on the computational and experimental analyses of a 3-DOF monolithic mechanism with a high resonant frequency. This mechanism consists of a monolithic structure with parallel flexure components to achieve all the three desired translational motions. Computational results and simulation are conducted using FEA software, ANSYS. A safety factor is calculated through computational analysis to show that the proposed mechanism can tolerate the total motion of the PEAs and confirm repeatability of the mechanism under maximum allowable stress of the proposed mechanism. An experimental study was conducted to investigate the dynamic and motion tracking performances of the proposed monolithic 3-DOF micromanipulator. Precise tracking performance is attainable by utilizing a feedback PI control methodology. A comparative investigation is conducted between the possessed resonant frequency of the proposed manipulator and the ones in the literature. The result of this comparison confirms that the proposed mechanism has good dynamic capabilities. Finally, the error analysis of the tracking performance of the proposed mechanism showed precise motion tracking and overall reliable performance.

2 Mechanism design

Figure 1 shows the isometric view of 3D model of the proposed monolithic 3-DOF micro/nano manipulator. This
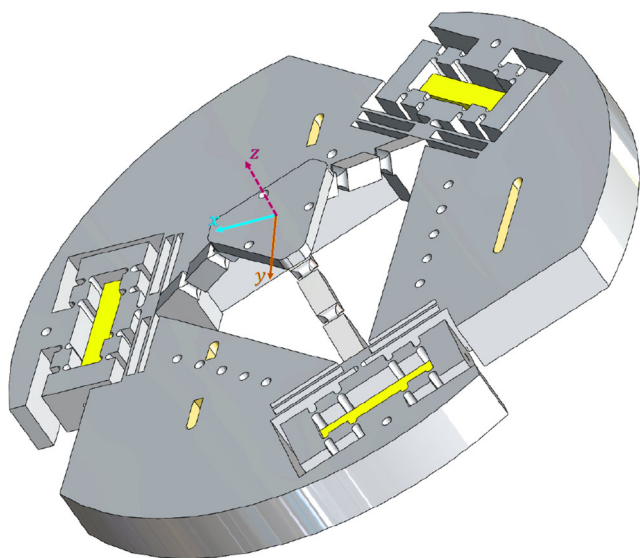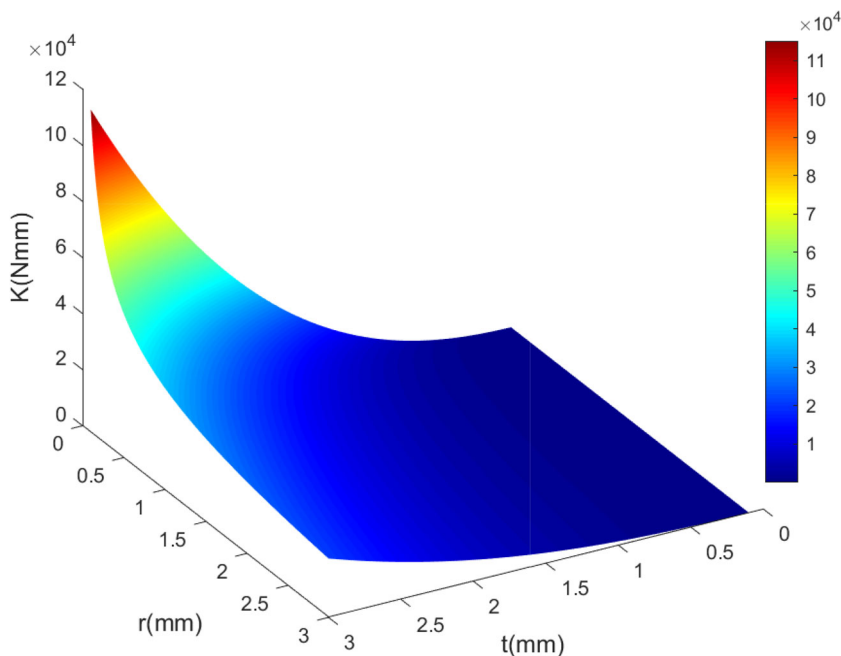
Fig. 1 Isometric view of 3D solid model of the monolithic 3-DOF parallel micromanipulator

mechanism consists of three bridge mechanisms connected to three leaf parallelogram mechanisms which are placed in a triangular configuration in the XY plane. The stage is connected to the in-plane mechanism by using three out-of-plane arms with each arm consisting two of universal joints. The leaf parallelogram mechanism allows the bridge mechanism to have an output only in the perpendicular direction to the leaf flexure. The function of the universal joints is to allow the arm to have bending at the point of each joint and preventing the arm to be subjected to torsion.

2.1 Circular hinge

Flexure hinges are basically used as the motion transfer components between different parts of the overall mechanism. Because of the small thicknesses they have makes it possible to have a monolithic structure without any conventional joints. However, maximum Von-Mises stress generally occurs in the flexure hinges of a mechanism as a result of having a small thickness. Different kinds of flexure hinges with different capabilities were introduced, but circular one was chosen to be used in this research due to its large applications in compliant micro-motion stages which required high precision of motions. Circular flexure hinges are precise in rotation where their center of rotations do not displace as much as other flexure hinges such as the left-type [31] and the corner-fillet [32]. Mathematically, circular flexure hinges are modelled as the revolute joints with constant torsional stiffness k_θ. The rotational stiffness and maximum nominal stress of a circular flexure hinge can be estimated and derived as;

$$k_\theta = \frac{2Ewr^2}{3f(\beta)} \tag{1}$$

$$\sigma_{max} = \frac{E(1+\beta)^{9/20}}{\beta^2 f(\beta)}, \beta = \frac{t}{2r} \tag{2}$$

where E, w, t, r are Young's modulus, out-of-plane thickness, in-plane thickness and hinge radius, respectively. θ_{max}

Fig. 2 Relationship between torsional stiffness, in-plane thickness and radius of circular hinges

Fig. 3 Relationship between Von-Mises stress, in-plane thickness and radius of circular hinges
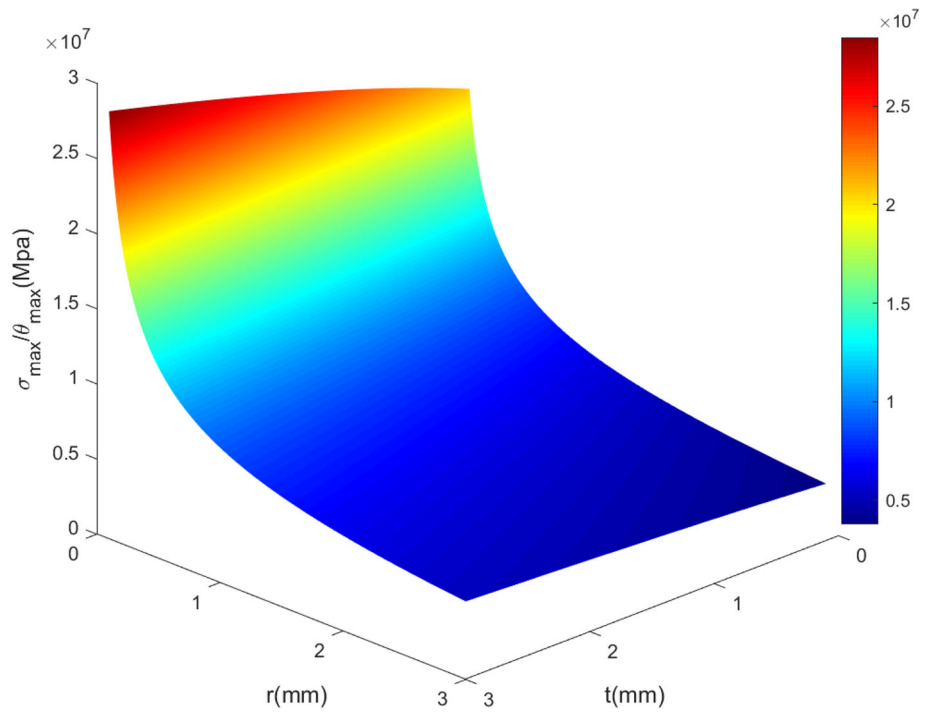
is the maximum rotational angle of hinges. In Eqs. 1 and 2, $f(\beta)$ is defined as follows;

$$f(\beta) = \frac{1}{\beta^2 + 2\beta} \left[\frac{2\beta^2 + 4\beta + 3}{(\beta + 1)(\beta^2 + 2\beta)} + \frac{6(\beta + 1)}{(\beta^2 + 2\beta)^{3/2}} \right.$$

$$\left. \times \tan^{-1}\left(\sqrt{\frac{\beta + 2}{\beta}}\right) \right] \qquad (3)$$

When the minimum thickness t is much smaller than the hinge radius r, the Eqs. 1 and 2 can be approximately given by;

$$k_\theta = \frac{2Ewt^{5/2}}{9\pi r^{1/2}} \qquad (4)$$

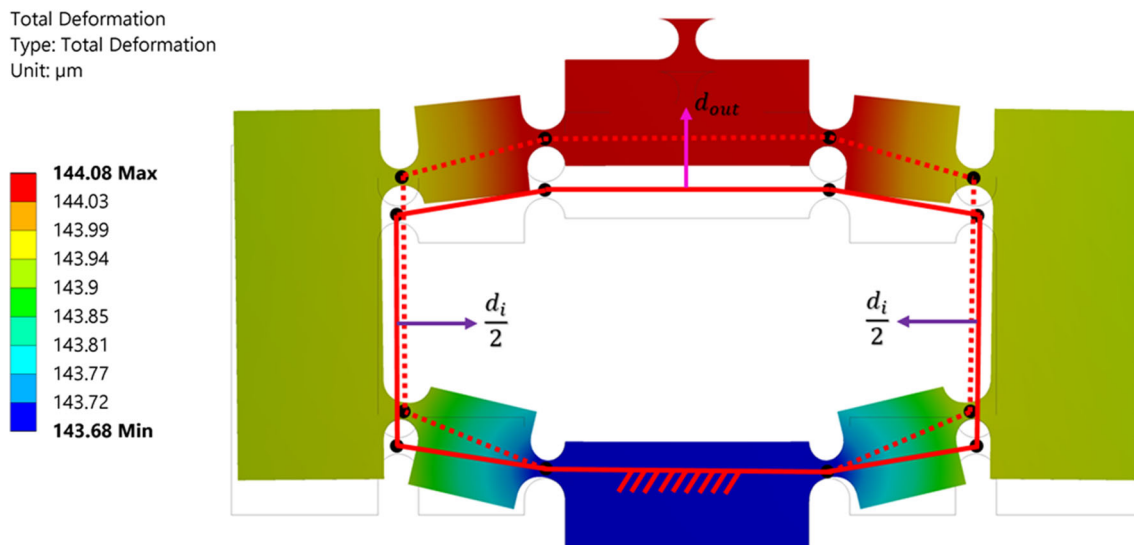$$\sigma_{max} = \frac{8}{3\pi} E(1 + \beta)^{9/20} \sqrt{\beta/2}\,\theta_{max} \qquad (5)$$

Fig. 4 Simulated model of a Bridge-type mechanism

Table 1 Physical and mechanical properties of ABS

Parameter	Value	Unit
Young's modulus (E)	2200	MPa
Tensile yield strength (σ_{yield})	31	MPa
Poisson's ratio (ν)	0.35	–
Density (ρ)	0.9087	g/cm^3

Maximum Von-Mises stress is an important factor in the designing and manufacturing. Surpassing the maximum stress from the yield strength, causes the mechanism to experience plasticity and deteriorates the system's performances and capabilities. Thus, during the design of the mechanism inequality (6) must be always considered;

$$\sigma_{max} \leqslant \sigma_{yield\ strength} \tag{6}$$

The relationship between torsional stiffness of circular flexure hinge, in-plane thickness and hinge radius is shown in Fig. 2. It can be noted that the in-plane thickness of a circular flexure hinge has direct relationship to the rotational stiffness, and the radius of hinge has inverse relationship. The effects of in-plane thickness and hinge radius on the ratio of maximum Von-Mises stress to maximum rotational angle of a circular flexure hinge is shown in Fig. 3. It is noted that the above-mentioned relationship is the same as the one that described for the rotational stiffness. In addition, the effect of radius is more dominant than the effect of in-plane thickness.

2.2 Bridge-type amplification mechanism

Bridge-type mechanism, rhombic mechanism, double-rocker mechanism, scott-russell mechanism, honey comb mechanism, and lever mechanism are a few amplification mechanisms which have been used for micro/nano manipulation purposes [33–37]. Among these mechanisms, the compliant bridge-type mechanisms, as shown in Fig. 4, have been widely used because of their compactness, symmetry and large magnification capability. In the last decade, compliant bridge-type mechanisms have been optimized regarding different application purposes and widely employed in flexure-based micro/nano manipulation mechanisms to provide amplified piezo-actuations. With the increasing

Table 2 Natural frequencies of the 3-DOF micromanipulator

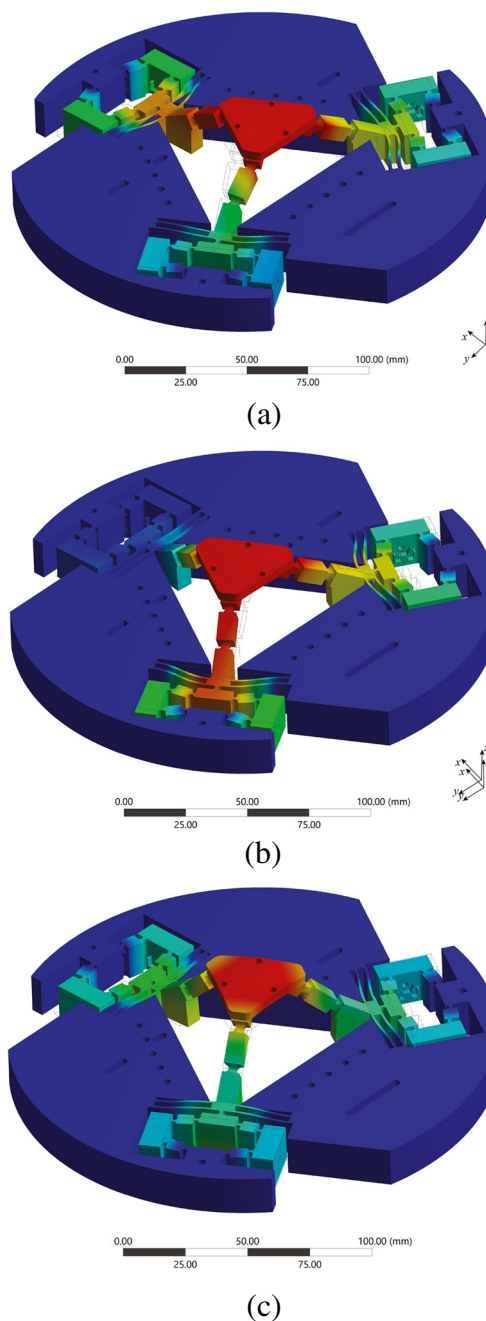| Mode No.	Frequency (Hz)
1	294.79
2	298.74
3	317.30

(a)

(b)

(c)

Fig. 5 Mode Shapes of the 3-DOF system **a** X translation (1st) **b** Y translation (2nd) **c** Z translation (3rd)

demands for high-dexterity manipulation, compliant bridge mechanisms have been used as a regular model to construct more complex structures with more DOF. Figure 4 shows a schematic of the motion of a one kind of bridge-type amplification mechanism under application of the load d_i. Each rigid beam and hinge are shown by a solid or dash line and a filled circle, respectively. Solid and dash lines show each limb and generally the bridge-type mechanism before and after application of the load. Therefore, the motion of each limb as a result of application of the load can be
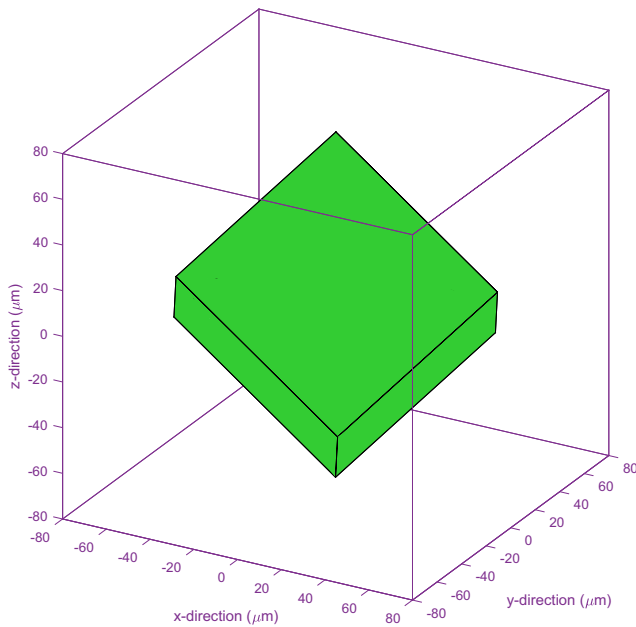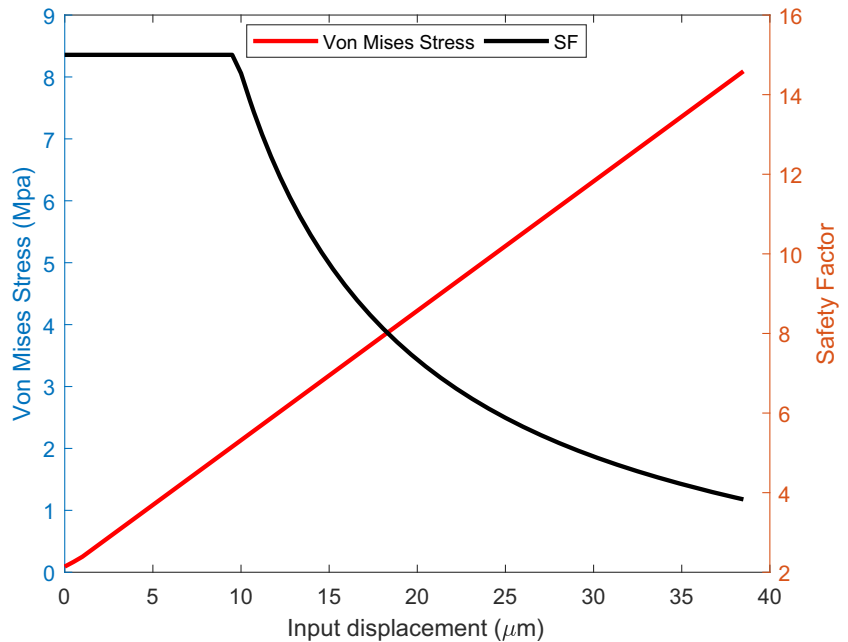
Fig. 6 3D simulated workspace of the monolithic parallel 3-DOF micromanipulator

seen. d_{out} shows the output of the bridge-type mechanism. The following relationship shows the amplification of a bridge-type mechanism;

$$Amp. = \frac{d_{out}}{d_{in}} \qquad (7)$$

For the specific bridge-type mechanism which is used in the proposed 3-DOF mechanism, the amplification is calculated as 3.74, using ANSYS.

3 Computational Analysis

By using FEA software (ANSYS), the behaviour of the proposed mechanism is investigated. During analysis, it was assumed that three PK4FYC2 Thorlabs PEAs were used with the maximum displacement of 38.5 μm under the input voltage of 150 V. The material, which is used for the purpose of the simulation, is Acrylonitrile Butadiene Styrene (ABS), and its properties are shown in Table 1.

Speed has become a critical issue in many micromanipulation applications, such as video-rate AFM and high throughput micro-manufacturing. One of the key limitations in speed is the systems mechanical resonance. As a result, designing a mechanical system to have the highest possible natural frequency is desired. Table 2 and Fig. 5 show the first three natural frequencies and the first three mode shapes of the proposed design, respectively. It can be seen that for the 3-DOF parallel mechanism the first natural frequency is 294.79Hz which is quite high and this confirms the repeatability and stability of the system.

Using FEA method, the computed Jacobian of the proposed design is established as follows;

$$J = \begin{pmatrix} -1.9193 & 0.9650 & 0.9577 \\ 0.0001 & 1.6651 & -1.6632 \\ 1.3975 & 1.2007 & 1.3309 \end{pmatrix}_{3\times3} \qquad (8)$$

Figure 6 shows the 3D workspace of the monolithic parallel 3-DOF micromanipulator. It is found to be $\pm 73.9579\mu m \times \pm 64.0705\mu m \times \pm 75.6340\mu m$, and the volume that is occupied by workspace is about $7.2E+05$ μm^3. The amplifications of the proposed mechanism along each axis are 3.84, 3.33 and 3.93, respectively.

Fig. 7 Effect of PEAs' input on the safety factor and Von-Mises stress

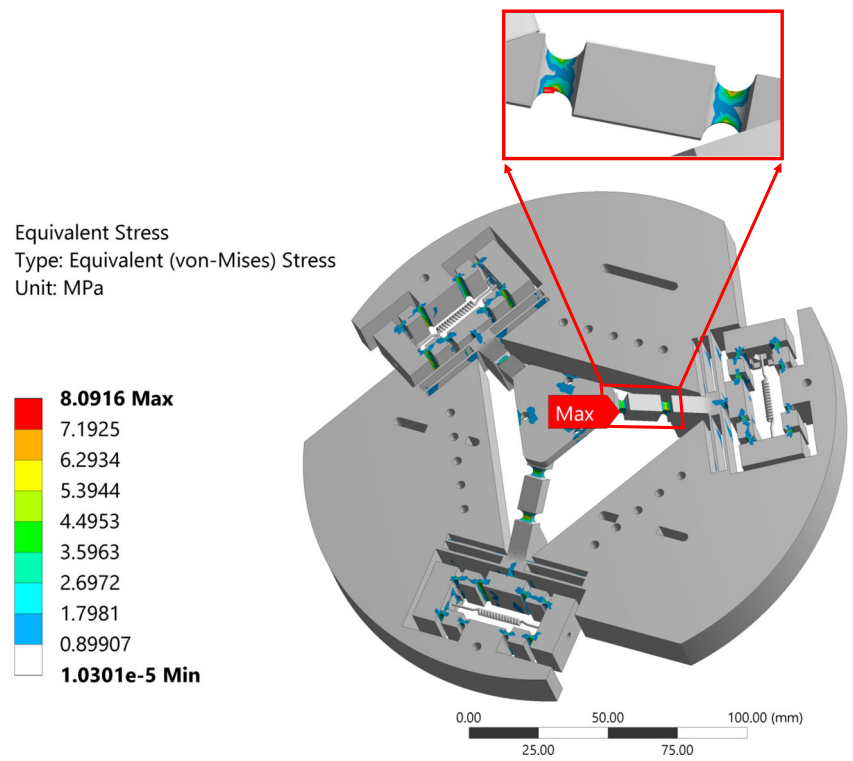**Fig. 8** Stress analysis investigation on the XYZ micromanipulator

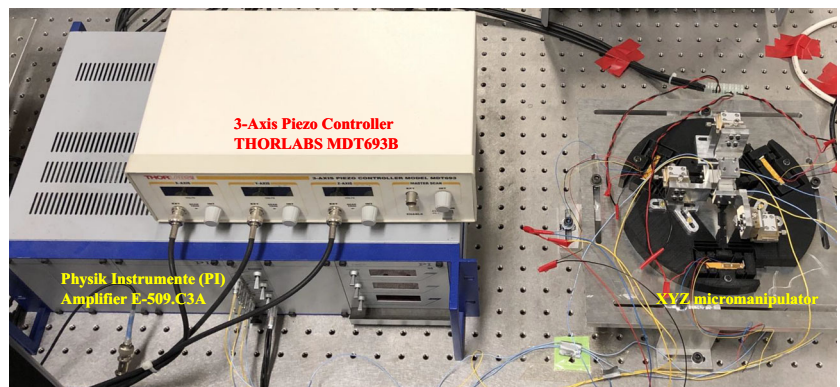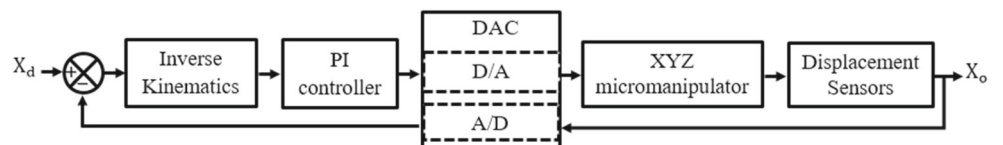**Fig. 9** Experimental setup of the 3-DOF XYZ micromanipulator

Fig. 10 Block diagram of control system for the proposed 3-DOF micromanipulator
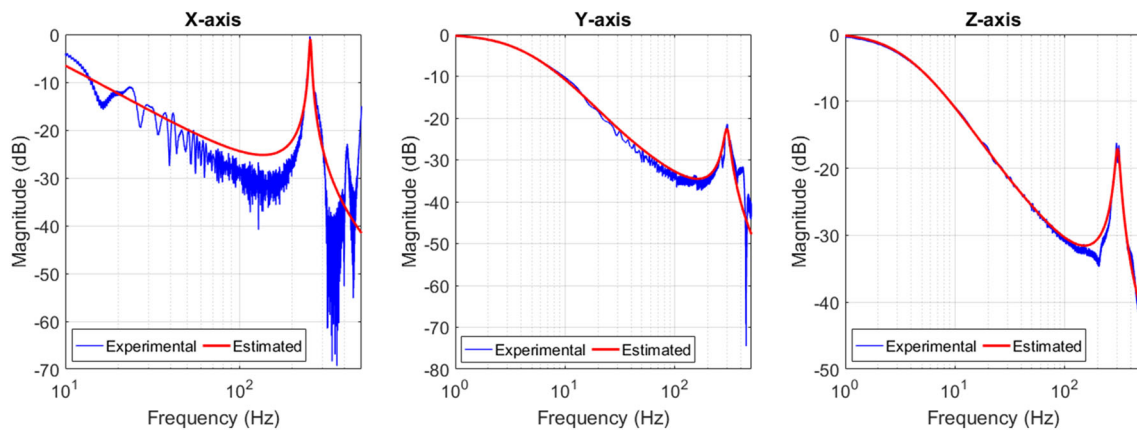
Fig. 11 Frequency response of the X, Y, and Z axes of the 3-DOF micromanipulator

It is necessary when designing a new structure to make sure that during the application of the load, it is not going to fail and/or surpass its yield strength, and it does not experience plasticity, as this will result in deterioration of the repeatability and capabilityof the system. Figure 7 shows the minimum safety factor and/or the maximum Von-Mises stress against PEA input. The best performance of a mechanical system's behaviour is achieved if the safety factor is satisfied. Equation 9 shows how the safety factor is determined;

$$Safety \; Factor \; (SF) = \frac{\sigma_{yield \; strength}}{\sigma_{max}} \qquad (9)$$

It is noted from Fig. 7 that the proposed system will never experience failure under the usage of this PEA, and stability and repeatability of the system will be guaranteed.

Figure 8 shows the Von-Mises stress analysis, which was performed using ANSYS. As it was predicted in Section 2.1, the maximum stress would occur at a thinnest part of a flexure hinge in a micro/nano manipulation mechanism. This trend is evident in Fig. 8 by the calculated maximum Von-Mises stress of 8.09 Mpa, which occurs in one of the universal joints. It can be seen in Fig. 7 that the minimum safety factor is 3.83, which occurs in the

same universal joint with the maximum Von-Mises stress. Therefore, the used universal joints are the most vulnerable parts of the designed mechanism. Furthermore, considering the obtained safety factor, it can be concluded that a higher input stroke can be applied and consequently a larger workspace can be achieved with the same design structure and parameters. However, for the proposed micromanipulator that possesses a high bandwidth frequency, the calculated workspace is significantly larger than the current existing piezo-driven flexure-based mechanisms.

4 Experimental study

In this section, a prototype of the proposed mechanism is fabricated monolithically using a 3D-printing technique and out of ABS and its performance is tested. A feedback controller, Proportional-Integral (PI), is implemented to force the manipulator to track a designed complex trajectory.

An overview of the experimental setup and platform are shown in Fig. 9. Fixed block of the compliant mechanism was mounted on an optical table to isolate the ground vibration. A real-time simulator with data acquisition system from Advantech was used to generate voltage signals and used to analyze the measured data. Power amplifier

Table 3 Comparison between the resonant frequency of the proposed micromanipulator and the previously existing structures

	First resonant frequency (Hz)		Material	DOF	Design characteristics
	FEA	EXP			
Bhagat et al. [19]	489.9	–	AL T7075	$XY\theta$	Non-monolithic & Planar
Guo et al. [20]	395.89	357.97	AL T7075	$XY\theta$	Monolithic & Planar
Al-jodah et al. [22]	109.37	–	ABS	$XY\theta$	Monolithic & Spatial
Xu and Li [29]	–	82	AL T7075	XYZ	Non-monolithic & Spatial
Tang and Chen [30]	80	–	AL T7075	XYZ	Non-monolithic & Spatial
Present	294.79	254.3	ABS	XYZ	Monolithic & Spatial

Fig. 12 The result of infinity trajectory tracking
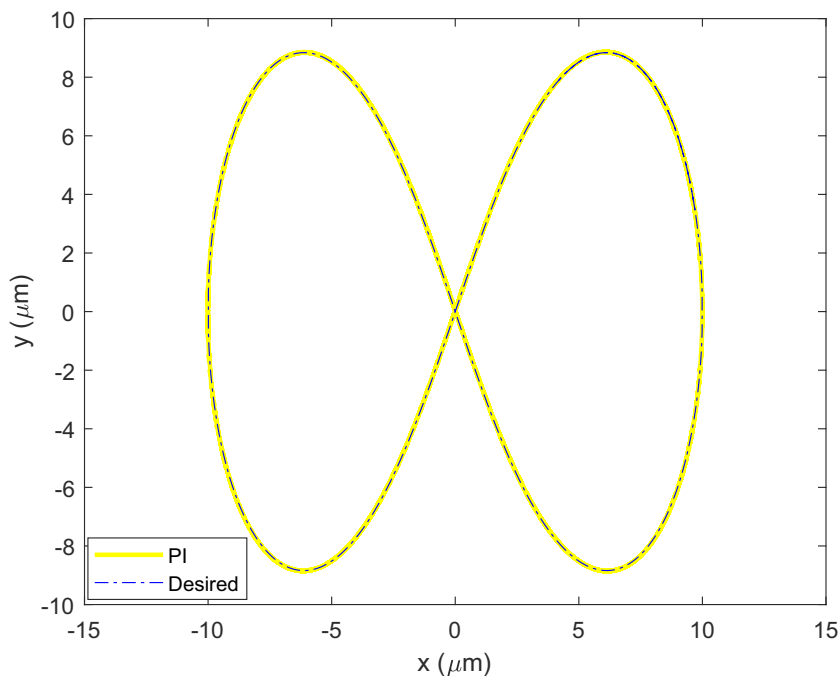
from Thorlabs was utilized to drive the piezo-stacks. Three Physik Instrumente capacitive sensors with a 50 μm measuring range were used to measure the output displacement. The feedback controller is a traditional PI controller used to compensate for environmental uncertainties and enhance stage stability. The schematic diagram of the feedback controller is shown in Fig. 10. $X_d = \begin{pmatrix} x_d & y_d & z_d \end{pmatrix}'$ and $X_o = \begin{pmatrix} cap - sensor_1 & cap - sensor_2 & cap - sensor_3 \end{pmatrix}'$ indicate the matrices of desired input motions and the output displacement of the micromanipulator from the capacitive sensors, respectively.

4.1 Modal testing

The modal analysis of the XYZ micromanipulator was identified by employing a sweep signal as the control input, which covers a frequency range from 1 Hz to 0.5 kHz. In this case, the output displacements were measured and recorded from 0 to 10 s. Figure 11 shows the frequency spectra of the stage's responses in the X, Y, and Z axes. Based on the frequency spectra, the natural frequencies of 254.3 Hz, 298.5 Hz, and 311.2 Hz were estimated along the X, Y, and Z axes, respectively. Natural frequencies of the manipulator decrease due to mounting instruments on the manipulator's stage. The stage was carring 25g apparatus at the time of capturing the manipulator's frequencies, therefore the actual mechanism's frequencies are higher than the captured ones.

As mentioned before, the proposed mechanism possesses a high natural frequency even though was made of ABS, a low stiff material. Table 3 shows a comparison between the proposed micromanipulator's first natural frequency and the reported ones in the literature. It is obvious from Table 3 that the present work shows better dynamic performances. It is worthy of mention that the natural frequencies of a mechanism have a direct relation to Young's modulus (E) of the material of that mechanism. Therefore, the larger E results in the higher natural frequencies. As a result, if the proposed micromanipulator was manufactured using AL T7075 and carring 25g apparatus, the first natural frequency would be 1236.3 Hz, which is comparable to the planar mechanisms in [19, 20].

4.2 Tracking performance

The motion of the 3-DOF system is coupled. Therefore, in order to eliminate this shortcoming, the inverse kinematics (J^{-1}, Eq. 8) is adopted in the feedback controller. Thus, each axis output of the system can be controlled independently when the system is controlled by the simultaneous control of three PEAs. Tracking performance of the 3-DOF flexure-based mechanism is tested to verify the performance and effectiveness of the developed control methodology. The tracking of an infinity trajectory and the corresponding tracking error along each axes are shown in Figs. 12 and 13, respectively. The maximum tracking errors of 0.19% and 0.66% along X and Y axes with respect to the motion range were attained. However, it is still possible to reduce this noise by using sensors with better performances.
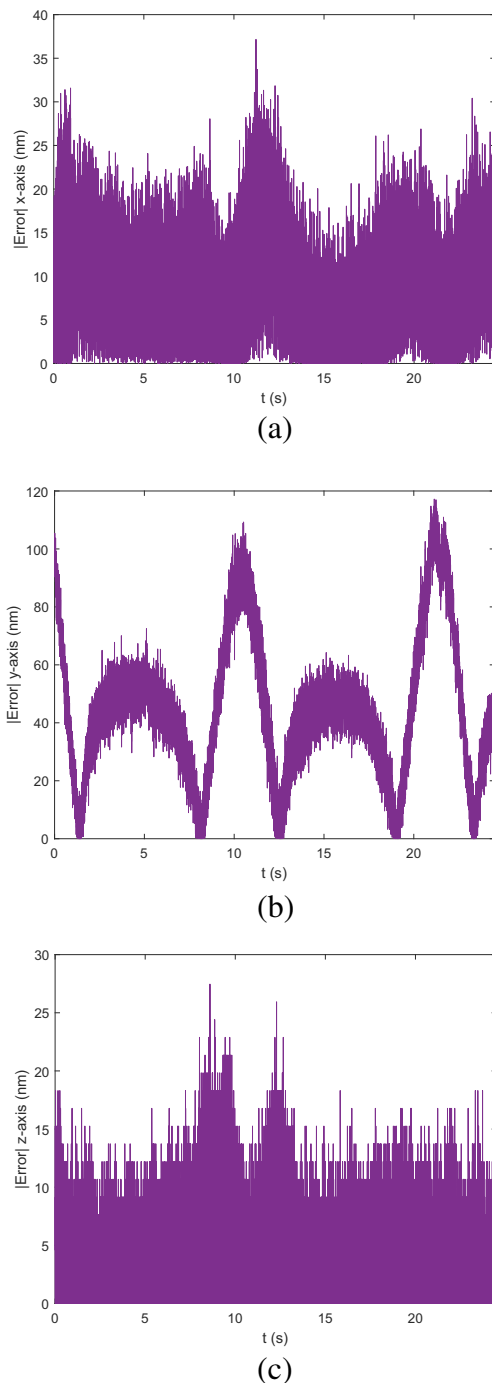
(a)

(b)

(c)

Fig. 13 The resultant error of infinity trajectory tracking; **a** x-axis **b** y-axis **c** z-axis

5 Conclusion

In this paper, a three DOF monolithic parallel piezo-driven micromanipulator with high bandwidth frequency was introduced. Computational and experimental analyses were conducted on this mechanism. The workspace was investigated and determined to be $\pm 73.9579 \mu$m$\times \pm$

64.0705μm$\times \pm 75.6340 \mu$m. The design structure provides a high dynamic bandwidth with the lowest natural frequency of 294.79Hz for the material of ABS. The mode shapes of the mechanism with the desired motion along each axis were determined and described. Moreover, stress analysis was performed on the mechanism and by using safety factor the stability of the mechanism was investigated. It was observed that even with the highest input of PEAs, safety factor remains higher than 1, which proves the stability of the mechanism. Finally, an experimental study was conducted on the proposed micromanipulator to investigate the claimed dynamic and precise motion performances. Therefore, a complex trajectory tracking (an infinity trajectory) was swept by the micromanipulator and the negligible observed trajectory tracking errors along each axes showed the effectiveness of the design and structure. Moreover, the frequency responses of the micromanipulator were obtained experimentally and a comparative investigation between the proposed mechanism's first resonant frequency and the existing ones were obtained to validate the computational results and the dynamic performances of the proposed XYZ micromanipulator.

References

1. Yang S, Maclachlan RA, Riviere CN (2015) Manipulator design and operation of a microsurgical instrument. IEEE/ASME Trans Mech 20(2):761–772
2. Yoshida S, Sato K, Takeuchi S (2013) Sequential micro-assembly of three dimensional biological microstructures from two dimensional cell-laden micro-plates. Procedia CIR 5(ii):196–200
3. Fukuda T, Arai F, Dong L (2003) Assembly of nanodevices with carbon nanotubes through nanorobotic manipulations. Proc IEEE 91(11):1803–1818
4. Shi C, Luu DK, Yang Q, Liu J, Chen J, Ru C, Xie S, Luo J, Ge J, Sun Y (2016) Recent advances in nanorobotic manipulation inside scanning electron microscopes, Microsystems and Nanoengineering, vol 2, no February
5. Pham MT, Teo TJ, Yeo SH (2017) Synthesis of multiple degrees-of-freedom spatial-motion compliant parallel mechanisms with desired stiffness and dynamics characteristics. Precis Eng 47:131–139
6. Pham MT, Teo TJ, Yeo SH, Wang P, Nai MLS (2017) A 3D-printed Ti-6Al-4V 3-DOF compliant parallel mechanism for high precision manipulation. IEEE/ASME Trans Mech 4435:1–10
7. Pham MT, Yeo SH, Teo TJ, Wang P, Nai MLS (2019) Design and optimization of a three degrees-of-freedom spatial motion compliant parallel mechanism with fully decoupled motion characteristics. J Mech Robot 11:1–8
8. Ghafarian M, Shirinzadeh B, Al-jodah A, Das TK, Wei W, Tian Y, Zhang D (2019) Design of a novel parallel monolithic 3-DOF

compliant micromanipulator. In: 2019 International Conference on Manipulation, Automation and Robotics at Small Scales (MARSS), pp 1–6

9. Xiao X, Li Y, Xiao S (2017) Development of a novel large stroke 2-DOF micromanipulator for micro/nano manipulation. Microsyst Technol 23(7):2993–3003

10. Su HJ, Shi H, Yu J (2012) A symbolic formulation for analytical compliance analysis and synthesis of flexure mechanisms. Journal of Mechanical Design, Transactions of the ASME 5: 134

11. Yong YK, Lu TF (2009) Comparison of circular flexure hinge design equations and the derivation of empirical stiffness formulations. IEEE/ASME International Conference on Advanced Intelligent Mechatronics, AIM 32:510–515

12. Zhu ZW, Zhou XQ, Wang RQ, Liu Q (2014) A simple compliance modeling method for flexure hinges. Sci China Technol Sci 58(1):56–63

13. Li Y, Xu Q (2007) Kinematic analysis of a 3-PRS parallel manipulator. Robot Comput Integr Manuf 23(4):395–408

14. Tang H, Li Y (2015) A new flexure-based $y\theta$ nanomanipulator with nanometer-scale resolution and millimeter-scale workspace. IEEE/ASME Trans Mech 20(3):1320–1330

15. Das T, Shirinzadeh B, Ghafarian M, Pinskier J (2018) A flexure-based 2-dof microgripper for handling micro-objects. In: MARSS 2018 - International Conference on Manipulation Automation and Robotics at Small Scales

16. Bhagat U, Shirinzadeh B, Clark L, Qin Y, Tian Y, Zhang D (2014) Experimental investigation of robust motion tracking control for a 2-DOF Flexure-Based mechanism. IEEE/ASME Trans Mech 19(6):1737–1745

17. Yang S, Chen W, Liu J, Chen W (2017) Design, analysis and testing of a novel decoupled 2-DOF flexure-based micropositioning stage. J Micromech Microeng 9:27

18. Zhu W-l, Zhu Z, Shi Y, Wang X, Guan K, Ju B-f (2016) Design, modeling, analysis and testing of a novel piezo-actuated XY compliant mechanism for large workspace nano- positioning. Smart Materials and Structures, no. 25

19. Bhagat U, Shirinzadeh B, Clark L, Chea P, Qin Y, Tian Y, Zhang D (2014) Design and analysis of a novel flexure-based 3-DOF mechanism. Mech Mach Theory 74:173–187

20. Guo Z, Tian Y, Liu C, Wang F, Liu X, Shirinzadeh B, Zhang D (2015) Design and control methodology of a 3-DOF flexure-based mechanism for micro/nano-positioning. Robot Comput Integr Manuf 32:93–105

21. Clark L, Shirinzadeh B, Tian Y, Yao B (2016) Development of a passive compliant mechanism for measurement of Micro/Nanoscale planar 3- DOF motions. IEEE/ASME Trans Mech 21(3):1222–1232

22. Al-jodah A, Shirinzadeh B, Ghafarian M, Tian Y, Clark L (2018) Design and analysis of a novel 3-DOF large range micropositioning mechanism. In: IEEE/ASME International Conference on Advanced Intelligent Mechatronics, AIM, vol 2018-July

23. Cai K, Tian Y, Wang F, Zhang D, Shirinzadeh B (2016) Development of a piezo-driven 3-DOF stage with T-shape flexible hinge mechanism. Robot Comput Integr Manuf 37:125–138

24. Ding B, Li Y, Xiao X, Tang Y, Li B (2017) Design and analysis of a 3- DOF planar micromanipulation stage with large rotational displacement for micromanipulation system. Mech Sci 8(1):117–126

25. Wang R, Zhang X (2017) Optimal design of a planar parallel 3-DOF nanopositioner with multi-objective. Mech Mach Theory 112:61–83

26. Qin Y, Shirinzadeh B, Zhang D, Tian Y (2013) Design and Kinematics Modeling of a Novel 3-DOF Monolithic Manipulator Featuring Improved Scott-Russell Mechanisms. J Mech Des 135(10):101004

27. Dong Y, Gao F, Yue Y (2016) Modeling and experimental study of a novel 3-RPR parallel micro-manipulator. Robot Com Int Manuf 37:115–124

28. Jensen KA, Lusk CP, Howell LL (2006) An XYZ Micromanipulator with three translational degrees of freedom. Robotica 24(3):305–314

29. Xu Q, Li Y (2012) Model predictive discrete-time sliding mode control of a nanopositioning piezostage without modeling hysteresis. IEEE Trans Control Syst Technol 20(4):983–994

30. Tang X, Chen IM (2006) A large-displacement 3-DOF flexure parallel mechanism with decoupled kinematics structure. In: IEEE International Conference on Intelligent Robots and Systems, pp 1668–1673

31. Tseytlin YM (2002) Notch flexure hinges: an effective theory. Rev Sci Instrum 73(9):3363

32. Lobontiu N, Paine JS, Garcia E, Goldfarb M (2001) Corner-filleted flexure hinges. Journal of Mechanical Design, Transactions of the ASME 123(3):346–352

33. Ghafarian M, Shirinzadeh B, Das T, Al-Jodah A, Wei W (2018) Design of a novel parallel monolithic 6-DOF compliant micromanipulation mechanism. In: IEEE/ASME International Conference on Advanced Intelligent Mechatronics, AIM, vol 2018-July

34. Clark L, Shirinzadeh B, Pinskier J, Tian Y, Zhang D (2018) Topology optimisation of bridge input structures with maximal amplification for design of flexure mechanisms. Mech Mach Theory 122:113–131

35. Chen J, Zhang C, Xu M, Zi Y, Zhang X (2015) Rhombic micro-displacement amplifier for piezoelectric actuator and its linear and hybrid model. Mech Syst Signal Process 50-51:580–593

36. Yang YL, Wei YD, Lou JQ, Tian G, Zhao XW, Fu L (2015) A new piezo-driven microgripper based on the double-rocker mechanism. Smart Mater Struct 24(7):75031

37. Muraoka M, Sanada S (2010) Displacement amplifier for piezoelectric actuator based on honeycomb link mechanism. Sensor Actuat A: Phys 157(1):84–90

Publisher's Note Springer Nature remains neutral with regard to jurisdictional claims in published maps and institutional affiliations.